PHYSICAL REVIEW B VOLUME 48, NUMBER 19 15 NOVEMBER 1993-I

Numerical transfer-matrix study of surface-tension anisotropy in Ising models on square and cubic lattices

Howard L. Richards
Supercomputer Computations Research Institute, Department of Physics, and Center for Materials Research and Technology, Florida State University, Tallahassee, Florida 32306-4052

M. A. Novotny
Supercomputer Computations Research Institute, Florida State University, Tallahassee, Florida 32306-4052

Per Arne Rikvold
Supercomputer Computations Research Institute, Department of Physics, and Center for Materials Research and Technology, Florida State University, Tallahassee, Florida 32306-4052

(Received 7 May 1993; revised manuscript received 9 July 1993)

We compute by numerical transfer-matrix methods the surface free energy $\tau(T)$, the surface stiffness coefficient $\kappa(T)$, and the step free energy $s(T)$ for Ising ferromagnets with $(\infty \times L)$ square-lattice and $(\infty \times L \times M)$ cubic-lattice geometries, into which an interface is introduced by imposing antiperiodic or plus/minus boundary conditions in one transverse direction. These quantities occur in expansions of the angle-dependent surface tension for either rough or smooth interfaces. The finite-size scaling behavior of the interfacial correlation length provides the means of investigating $\tau(T)$, $\kappa(T)$, and $s(T)$. The resulting transfer-matrix estimates are fully consistent with previous series and Monte Carlo studies, although current computational technology does not permit transfer-matrix studies of sufficiently large systems to show quantitative improvement over the previous estimates.

I. INTRODUCTION

Many phenomena of interest in condensed-matter physics, materials science, and high-energy physics occur in systems in which two or more thermodynamic phases coexist below some critical temperature T_c. These phenomena are strongly influenced by the behavior of interfaces between the phases. Examples of interfacial phenomena from condensed-matter physics include wetting, nucleation and growth, and crystal faceting. An example from high-energy physics is spatially nonuniform symmetry-breaking in the early universe. A number of these systems also have a *roughening transition* at a temperature T_R (known as the roughening temperature), at which the interface changes from microscopically flat to microscopically rugged.[1,2] For the three-dimensional (3D) cubic-lattice Ising model, a recent Monte Carlo study yields $T_R = 2.454\,59(5)J/k_B$.[3] This is consistent with an earlier Monte Carlo estimate $T_R = 0.542(5)T_c = 2.45(2)J/k_B$,[4] where a Monte Carlo renormalization-group estimate for the critical temperature,[5] $T_c = 4.511\,576\,7(2)J/k_B$, has been used. The roughening transition of one exactly solvable solid-on-solid (SOS) model[6] has been shown to belong to the Kosterlitz-Thouless (KT) universality class,[7,8] and roughening transitions in related SOS models and in the 3D Ising model are generally believed to belong to this universality class as well.[1] On the other hand, for the two-dimensional (2D) square-lattice Ising model $T_R = 0$; that is, the interface is always rough.

An aspect of interfaces that is of great importance in determining interface profiles and dynamics is the surface tension, which is the amount by which each unit area of interface increases the total free energy of the system in the thermodynamic limit.[9] A great deal of analytical work,[10–13] including low-temperature series expansions,[14–16] has been done to study interfaces and their associated surface tensions. The surface tensions in a ϕ^4 field theory[17] and in the q-state Potts model[18,19] have been studied by Monte Carlo simulations. Of particular interest has been the dependence of the surface tension in the 2D and 3D Ising models on the orientation of the interface relative to the underlying lattice (see Fig. 1); this has been studied both analytically[20–22] and through Monte Carlo simulations.[4,17,23–28]

The analytical treatments of the 3D Ising model rely on approximations which are perturbative in nature, whereas the nonperturbative Monte Carlo method suffers from critical slowing-down and the possibility of becoming trapped in metastable or long-lived unstable states. Furthermore, free energies and correlation lengths are cumbersome to calculate in Monte Carlo simulations. Although sophisticated techniques, such as cluster algorithms[3,29] and the multicanonical ensemble,[28,30] have been developed to circumvent most of these difficulties (particularly for simple models like the Ising model), a simple alternative method, which has been successful in the study of phase transitions, particularly in 2D systems, is that of numerical transfer-matrix (TM) calculations combined with finite-size-scaling (FSS) analysis.[31]

0163-1829/93/48(19)/14584(15)/$06.00

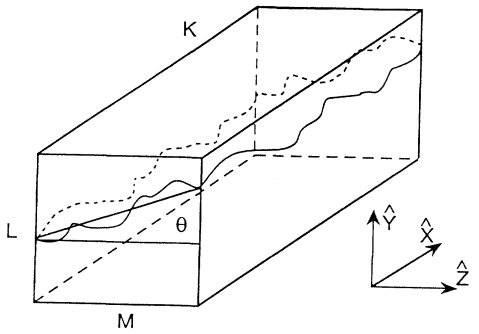

FIG. 1. A 3D system illustrating the axes and dimensions of the system, and the orientation of the interface, which separates the region of positive magnetization from the region of negative magnetization. In this figure boundary conditions are used to tilt the interface by a fixed angle θ with respect to the z direction. Although the boundary conditions discussed in the text do not produce such a tilt, they can be used to predict the change a tilt would produce in the surface tension.

The numerical TM FSS method does not encounter the aforementioned difficulties: (i) It is nonperturbative and does not require foreknowledge of special temperatures (such as T_R and T_c) or of critical exponents; (ii) it has no dynamics, so that critical slowing down does not occur and the equilibrium state is readily found; (iii) the free energy corresponds to the largest eigenvalue of the TM, and so is readily found; (iv) the calculations are actually *easier* if the length of the system in one direction is infinite; and (v) the correlation length in this direction is simple to find since only the two largest eigenvalues of the TM are required. For these reasons, there has recently been renewed interest in calculating interfacial properties by TM techniques.

Nevertheless, because the order of the TM increases exponentially with the number of sites in a transverse layer (discussed quantitatively in Sec. II), the size of systems which can be investigated through the numerical diagonalization of a TM is greatly limited. As a result, FSS analysis is even more important for TM calculations than for Monte Carlo simulations. The order of the TM has also limited most previous attempts at calculating the surface-tension anisotropy by TM techniques to capillary-wave and SOS approximations.[21,22,32] Specifically, in Refs. 21 and 22 Privman and Švrakić derived FSS relations for the correlation length of the Ising model in two and three dimensions by using capillary-wave and SOS approximations; these scaling relations involve the surface-tension anisotropy. The scaling relations for the 3D model were derived through comparison with the 2D Ising model, which has been solved exactly[33–36] for the boundary conditions used in Refs. 21 and 22 to generate an interface. In the rough phase, a longitudinal cross-section perpendicular to the interface was compared with a 2D system, whereas in the smooth phase the interface itself was compared with a 2D system.

In this article we present a large-scale numerical TM FSS study of surface-tension anisotropy in 2D and 3D Ising models. The analytic scaling relations of Privman and Švrakić[21,22] are applied to analyze free energies and correlation lengths obtained by numerical diagonalization of transfer matrices describing Ising models on both $\infty \times L$ square lattices and $\infty \times L \times M$ cubic lattices[37] into which an interface along the longitudinal (x) direction can be introduced by applying appropriate boundary conditions (discussed in Sec. II) in the y direction. The purpose of this study is threefold: (i) to test the analytically obtained scaling relations and possibly identify extensions or corrections, (ii) to investigate whether the limits on system size imposed by the present generation of parallel and vector supercomputers and diagonalization algorithms allow us to reach the asymptotic scaling regime in which FSS relations can yield information about interfacial properties in the thermodynamic limit, (iii) to compare the resulting estimates of interfacial properties with estimates previously obtained by other analytical and numerical methods. Throughout this study we use the full Ising model, which includes contributions from microstates with bubbles and overhangs as well as SOS microstates.

We now define the quantities to be studied in this work. Given an interface (see Fig. 1) making only a small angle θ with the xz plane, the surface tension $\sigma(\theta,T)$, measured per unit projected area in the xz plane, has a series expansion for $T > T_R$,[38]

$$\sigma(\theta,T)/\cos\theta = \tau(T) + \frac{1}{2}\kappa(T)\theta^2 + O(\theta^4) . \tag{1}$$

The coefficients in this expansion are the surface free energy

$$\tau(T) = \sigma(0,T) > 0 \tag{2}$$

and the surface stiffness coefficient

$$\kappa(T) = \sigma(0,T) + \left.\frac{\partial^2\sigma(\theta,T)}{\partial\theta^2}\right|_{\theta=0} . \tag{3}$$

If $T < T_R$, $\kappa(T)$ is infinite, and the system can gain entropy only through microscopic fluctuations (i.e., fluctuations on a length scale much shorter than the mesoscopic capillary waves), among which single-step terraces are dominant. Each single-step terrace contributes a quantity $s(T)$, which is nonzero below T_R, to the total free energy of the system; this quantity is known as the step free energy. The step free energy is measured per unit length of the total perimeter of all the terraces. The step free energy can also be related to the surface tension per unit projected area by an expansion when $T < T_R$:[39]

$$\sigma(\theta,T)/\cos\theta = \tau(T) + s(T)|\theta| + O(\theta^2) . \tag{4}$$

The anisotropy of the free energy will be discussed in terms of these three quantities: $\tau(T)$, $\kappa(T)$, and $s(T)$.

The remainder of this paper is organized as follows. We define the model and discuss the appropriate boundary conditions in Sec. II. In Sec. III we discuss estimates of the surface free energy. Section IV contains estimates of the surface stiffness coefficient, and Sec. V

is devoted to the step free energy. In Sec. VI we use the Roomany-Wyld approximant for the Callan-Symanzik β function[40,41] to study the scaling of the correlation length, especially near the roughening temperature. Our results are summarized and discussed in Sec. VII.

II. MODEL AND METHODS

We study the ferromagnetic Ising model with square and cubic lattice geometries. Each site i has a spin $s_i = \pm 1$, which interacts with the spin at each nearest-neighbor site j with an interaction constant $J_{i,j} > 0$. The Hamiltonian for this system is given by

$$\mathcal{H} = -\sum_{\langle i,j \rangle} J_{i,j} s_i s_j - \sum_{(i)} h_i s_i \ . \tag{5}$$

Here $\langle i,j \rangle$ denotes nearest-neighbor pairs on a periodic lattice, and (i) represents boundary sites. For nearest-neighbor pairs not on a boundary, $J_{i,j} = J$. Throughout this article the lattice constant is of unit length.

Various boundary conditions are needed to prepare both systems with interfaces and systems without interfaces. A transverse layer in a 2D system consists of a 1D lattice with L sites in the y direction, and in 3D a layer is a 2D lattice with L sites in the y direction and M sites in the z direction. The presence or absence of an interface is determined by conditions on the boundaries $y = 1$ and L. All systems we study have the following: (i) a boundary interaction constant J_y connecting the site at $(x,\ y = 1,\ z)$ with the site at $(x,\ y = L,\ z)$, (ii) a lower-boundary magnetic field h_1 applied on the $y = 1$ plane, and (iii) an upper-boundary magnetic field h_L applied on the $y = L$ plane. Table I summarizes the five types of boundary conditions used in this paper.

TABLE I. Boundary conditions discussed in the text.

Name	J_y	h_1	h_L
Free	0	0	0
Periodic	J	0	0
Antiperiodic	$-J$	0	0
Plus/plus	0	J	J
Plus/minus	0	J	$-J$

It should be noted that the "width" of systems with plus/plus and plus/minus boundary conditions can be defined by measuring different quantities. These boundary conditions can be imposed by coupling the planes at $y = 1$ and at $y = L$ to planes of fixed spins. In this case there are $L+1$ couplings in the y direction, and this number is often used instead of the number L of spin sites as the measure of system width (for example, in Refs. 21, 22, and 36). In this article width refers to the number of sites L.

A transfer matrix $\underline{T}$ can be used to find the free energy per unit length in the longitudinal direction. In our case $\underline{T}$ can be chosen to be symmetric, in which case the transfer matrix is explicitly the $2^A \times 2^A$ matrix

$$\langle s_1, \ldots, s_A | \underline{T} | s'_1, \ldots, s'_A \rangle = \prod_{\langle i,j \rangle} \exp(J_{i,j}[s_i s_j + s'_i s'_j]/2k_BT) \prod_{(i)} \exp(h_i[s_i + s'_i]/2k_BT) \prod_i \exp(J s_i s'_i / k_BT) \ , \tag{6}$$

where the area A of a transverse layer is given by $A = L$ in 2D and by $A = LM$ in 3D. Here the spins s_i and s'_i are in adjacent layers. The interactions within a layer are taken into account in the first and second products of Eq. (6), and $\langle i,j \rangle$ and (i) denote nearest-neighbor pairs and boundary sites, respectively, within the given layer. The third product of Eq. (6) takes into account nearest-neighbor interactions in the transfer direction. The largest eigenvalue of $\underline{T}$, Λ_0, is related to the partition function Z in the limit of infinite longitudinal size $(K \to \infty)$ by[31,42–45]

$$\lim_{K\to\infty} Z^{1/K} = \lim_{K\to\infty} \left(\mathrm{Tr}\left[\underline{T}^K\right] \right)^{1/K} = \Lambda_0 \ . \tag{7}$$

Using the thermodynamics of the canonical ensemble, Eq. (7) can be used to find quantities such as the free energy per site,

$$f = \frac{-k_BT}{A} \ln \Lambda_0 \ . \tag{8}$$

The longitudinal correlation length is given by the ratio of the largest and next-largest eigenvalues of $\underline{T}$:

$$\xi = 1/\ln|\Lambda_0/\Lambda_1| \ . \tag{9}$$

Other length scales can be defined from smaller eigenvalues of $\underline{T}$, and scaling *Ansätze* analogous to those we use in the next two sections have been proposed[21,22] for these length scales. Here we consider only the correlation length defined by Eq. (9), since it is expected that the other length scales require larger values of L (and in 3D, M) to scale in the asymptotic fashion.

For the Ising model, exact solutions have been found for the free energy and correlation length in finite 2D systems with antiperiodic boundary conditions[34] or plus/minus boundary conditions,[35,36] so that systems with arbitrarily large values of L can be used in FSS. In 3D, on the other hand, numerical diagonalization of the large matrix $\underline{T}$ restricts us to small values of A due to limited computer memory. We are able to study cross sections as large as $A = 19$ on a Cray Y-MP/432 computer by using the Numerical Algorithms Group (NAG) diagonalization routine F02FJE. The largest cross section we can study is $A = 25$, for which an eigenvector of $\underline{T}$ has 33 554 432 elements. Such large systems were run on a Thinking Machines Corporation CM2 computer using a modified power algorithm[46] (for details see Appendix A). We estimate that about 125 h on the Y-MP and 700 h on the CM2 were used for the numerical calculations in this article.

III. THE SURFACE FREE ENERGY

In order to estimate the surface free energy from finite systems, we compare the free energy of two similar systems, one of which has an interface and one of which does not. We attribute the difference to the interface. Specifically, we estimate τ from antiperiodic (a) and periodic (p) boundary conditions in the y direction by[10–12,22]

$$\tau_L^a(T) \equiv L(f_L^{(a)}(T) - f_L^{(p)}(T)), \tag{10}$$

and from plus/minus (+/−) and plus/plus (+/+) boundary conditions in the y direction by[10–12,22]

$$\tau_L^{(+/-)}(T) \equiv L(f_L^{(+/-)}(T) - f_L^{(+/+)}(T)). \tag{11}$$

The factor L, which is the width of the system perpendicular to the interface, is needed to convert the difference between the volume densities f into a surface density. These relations provide just one possible definition of the surface tension in the 2D Ising model, but it has been proven[47] that all such definitions are equivalent with that of Onsager for low temperatures. These estimates are valid in any number of dimensions (in 3D the subscript L is replaced by L, M).

Figure 2(a) shows the 2D estimates $\tau_L^a(T)$ defined in Eq. (10) and the exact solution $\tau(T)$ in the infinite-lattice limit.[33] The difference between the finite-size estimate and the infinite limit in this case is inversely proportional to the correlation length in the periodic system, so that for $T < T_c$, $\tau_L(T)$ converges to $\tau(T)$ exponentially with L.[34] Thus the size dependence is noticeable only near T_c; in all cases, for 2D it has been shown[48] that the critical-point behavior is such that $\sigma(T)$ vanishes linearly with the reduced temperature, $t \equiv (T_c - T)/T_c$.

The 2D estimates $\tau_L^{(+/-)}(T)$ defined in Eq. (11) are plotted in Fig. 2(b). In this case, however, we observe numerically that the estimates from finite-width lattices converge as a simple power law:

$$\tau_L^{(+/-)}(T) - \tau(T) \approx A(T)L^{-B}. \tag{12}$$

The effective scaling exponent is thus given by

$$B(L,T) = -\frac{d\ln[\tau_L^{(+/-)}(T) - \tau(T)]}{d\ln L}, \tag{13}$$

where the derivative is calculated by multiple-point finite differences. By holding $T = T_c$ and calculating $\tau_L^{(+/-)}(T)$ for values of $L = 2^i \times 10$, $i \in \{1, 2, \ldots, 15\}$, we can use Aitken's Δ^2 method[49] to find $\lim_{L\to\infty} |B(L,T_c) - 1| < 10^{-9}$, in agreement with the prediction $\lim_{L\to\infty} B(L,T_c) = 1$.[31] Using the same method but fixing $k_BT = 1.5J$, we find that for $T < T_c$, $|\lim_{L\to\infty} B(L,T) - 2| < 10^{-7}$. For $T \leq T_c$ and large L, the scaling exponent B is observed numerically to be a function only of the critical scaling variable $tL^{1/\nu} = tL$ (Fig. 3).

The estimates $\tau_{L,M}^a(T)$ for 3D are graphed in Fig. 4(a). Again the convergence appears to be quite rapid except near T_c. Similar rapid convergence is seen in the estimate $\tau_{L,M}^{(+/-)}(T)$ for 3D [Fig. 4(b)]. The value of $\tau(T)$ is exactly known for 3D only at $T = T_c$ (where $\tau = 0$) and at $T = 0$ (where $\tau = 2J$), but estimates from series expansions im-

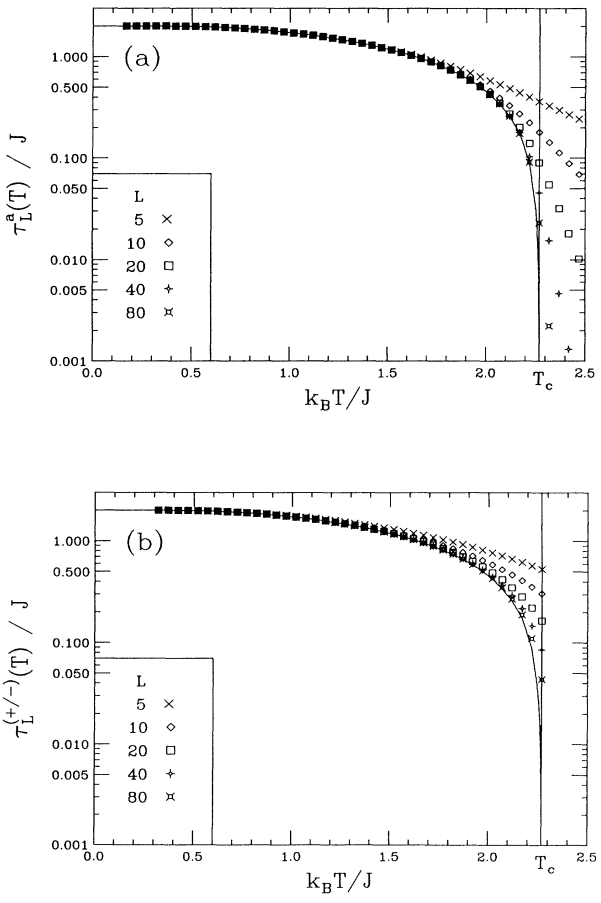

FIG. 2. The estimates of the surface free energy in two dimensions. (a) $\tau_L^a(T)$, from Eq. (10), and (b) $\tau_L^{(+/-)}(T)$, from Eq. (11). The solid curve is the limit of $\tau_L(T)$ for an infinite lattice (Ref. 33). The solid vertical line gives the 2D critical temperature.

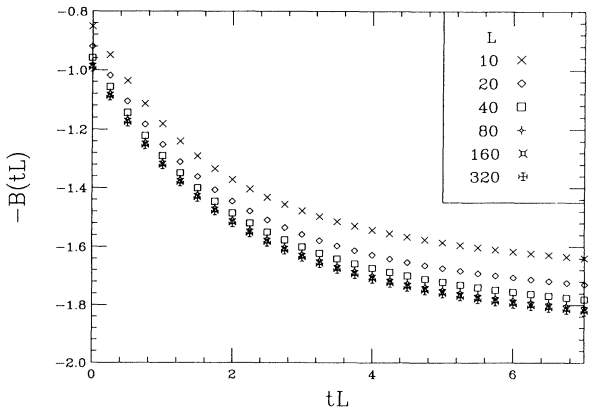

FIG. 3. The effective scaling exponent $B(tL)$ for $\tau_L^{(+/-)}(T)$ in two dimensions, defined in Eq. (13) and evaluated by numerical differentiation.

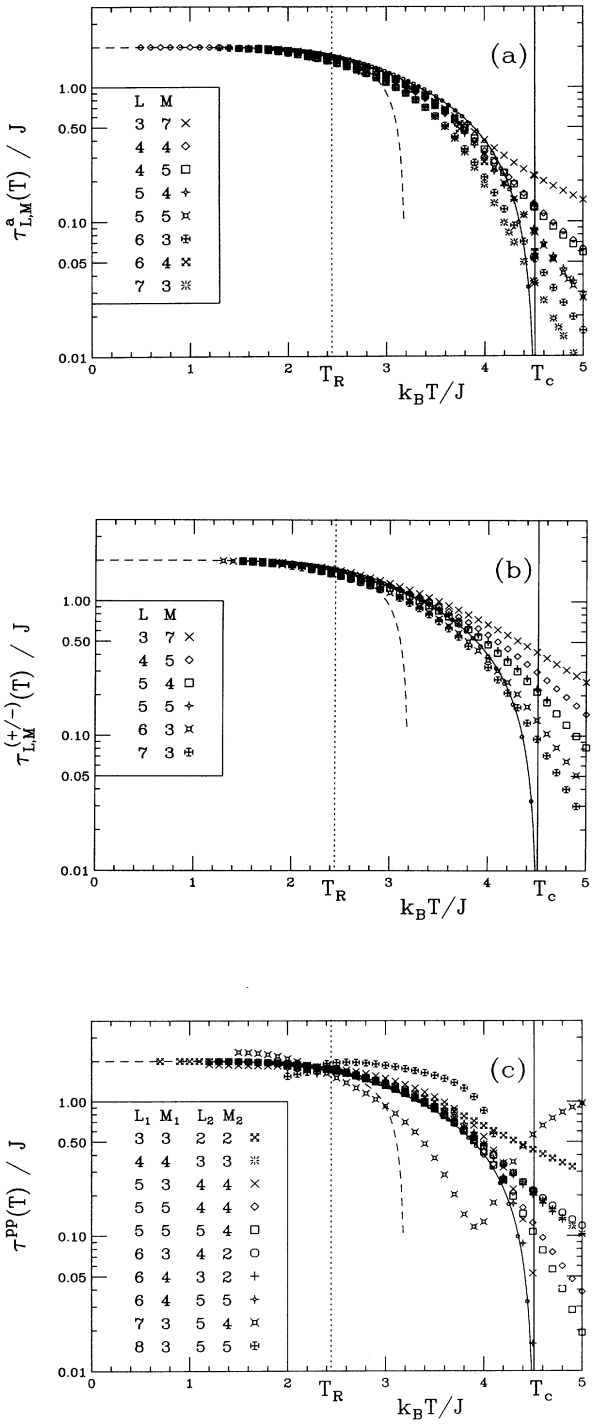

FIG. 4. The estimates of the surface free energy in three dimensions. (a) $\tau^a_{L,M}(T)$, from Eq. (10), and (b) $\tau^{(+/-)}_{L,M}(T)$, from Eq. (11), (c) $\tau^{pp}(T)$, from Eq. (16). The dashed curve is a low-temperature expansion (Ref. 16), the solid curve comes from series expansion improved with Padé approximants (Ref. 50), and small solid circles (bigger than the error bars) indicate the results of Monte Carlo simulations (Ref. 27). The vertical dotted line indicates the roughening temperature, T_R, as determined from Monte Carlo studies (Ref. 3). The solid vertical line marks the 3D critical temperature as determined by a Monte Carlo Renormalization Group study (Ref. 5).

proved with Padé approximants[50] and from Monte Carlo simulations[27] agree well with our $L \approx M$ results. At T_c, $\tau^a_{L,M}$ appears to converge to zero as L^{-2} with little dependence on M, but it is difficult to be certain with only a few small systems. Recent analytic results[51] for cubic ($K = L = M$) systems with antiperiodic boundary conditions indicate that the asymptotic scaling region is reached only with very large systems.

An alternative method for estimating the surface free energy in three dimensions uses two systems with periodic boundary conditions in both the y and z directions.[26,52] In this case the surfaces are domain walls perpendicular to the transfer direction. The correlation length follows the scaling relation[26,52,53]

$$\xi^p_{L,M} \approx \exp[\tau(T)LM/k_BT]/Z_{\rm cw}(L,M)\ , \tag{14}$$

where[54,55]

$$Z_{\rm cw}(L,M) = \widetilde{C}(T)\sqrt{\frac{M}{L}}q^{-12}\ (1+q+2q^2+3q^3+5q^4 +7q^5+11q^6+\cdots)^2\ . \tag{15}$$

Here $\widetilde{C}(T)$ is an undetermined function of temperature, $q \equiv \exp(-2\pi L/M)$, and $L \geq M$. Equation (14) can be solved for $\tau(T)$ if the correlation lengths of two different systems are known:

$$\tau^{pp}(T) = k_BT\frac{\ln \Xi^p(L_1,M_1,T) - \ln \Xi^p(L_2,M_2,T)}{L_1M_1 - L_2M_2}\ , \tag{16}$$

where $\Xi^p(L,M,T) = \xi^p_{L,M}Z_{\rm cw}(L,M)$. As can be seen in Fig. 4(c), this estimate converges rapidly for $T < T_c$, particularly when $L_1/M_1 = L_2/M_2$. In that case it appears that $\tau(T)$ is always overestimated, whereas the estimates $\tau^a_{L,M}(T)$ crosses $\tau(T)$ at a temperature which depends on the system size. It is also worth pointing out that although $Z_{\rm cw}(L,M)$ is canceled out in Eq. (16) when $L_1/M_1 = L_2/M_2$, it is important in other cases, as we have observed by trying $Z_{\rm cw}(L,M) = \text{const}$.

IV. THE SURFACE STIFFNESS COEFFICIENT

A. κ in two dimensions

A capillary-wave calculation[21,22] yields that the correlation length for antiperiodic boundary conditions and large L should scale as

$$\xi^a_L(T) \approx \frac{2}{\pi^2}\frac{\kappa(T)}{k_BT}L^2 \tag{17}$$

for all $T < T_c$. Solving this equation for $\kappa(T)$ gives a finite-size estimate for the surface stiffness coefficient,

$$\kappa^a_L(T) = k_BT\frac{\pi^2}{2}\frac{\xi^a_L(T)}{L^2}. \tag{18}$$

Exact results[56] agree with this relation to leading order in L.[34] This estimate is shown in Fig. 5(a), as is the exact solution in the infinite-lattice limit.[34] We have analyzed the convergence and found that for temperatures $T \leq T_c$

the finite-lattice estimate converges to its infinite-lattice limit in a simple power-law fashion:

$$\kappa_L^a(T) - \kappa(T) \approx aL^{-b}. \tag{19}$$

As in Sec. III, we use multiple-point numerical differentiation to determine an effective scaling exponent

$$b(L,T) = -\frac{d\ln[\kappa_L^a(T) - \kappa(T)]}{d\ln L}, \tag{20}$$

which is displayed in Fig. 6(a). Although b is not monotonic, it shares the most important characteristics of the scaling exponent B defined in Eq. (13); that is, b varies from $b=1$ for $T=T_c$ (in agreement with critical scaling) to $b=2$ for $T \ll T_c$, and b is a function only of the critical scaling variable tL for large L.

The exact solution for $[\xi_L^a(T)]^{-1}$ is a sum in which both the total number of terms and each individual term depends on L.[34] We avoid the resulting difficulty of exactly differentiating $\kappa_L^a(T)$ with respect to L by using numerical differentiation in the evaluation of Eq. (20). However, it is also possible to define a "reduced correlation length" $\hat{\xi}(T)$, obtained from the antiperiodic correlation length $\xi^a(T)$ and the periodic correlation length $\xi^p(T)$ by

$$[\hat{\xi}_L(T)]^{-1} = [\xi_L^a(T)]^{-1} + [\xi_L^p(T)]^{-1}, \tag{21}$$

which contains only one explicitly L-dependent term [see Eq. (B7) in Appendix B]. Replacing $\xi_L^a(T)$ in Eq. (18) with $\hat{\xi}_L(T)$, we find an estimate, $\hat{\kappa}_L(T)$, which is a differentiable function of $\ln(L)$ if L is treated as a continuous variable. Except for small systems or $T \approx T_c$, $[\xi_L^p(T)]^{-1}$ is vanishingly small in comparison with $[\xi_L^a(T)]^{-1}$. Thus it is clear that $\hat{\kappa}_L(T)$ will be less than $\kappa_L^a(T)$ but must converge to the same limit. In fact, for all L, $\kappa(T) < \hat{\kappa}_L(T) < \kappa_L^a(T)$. In the limit of large L we find the effective scaling exponent

$$\hat{b}(tL) = 2\left(\frac{1}{1 - 4c(tL)^2[g(tL) - 2c]/\pi^2}\right) \times \left(1 - \frac{\pi^2}{2(tL)^2 g(tL)[g(tL) - 2c]}\right), \tag{22a}$$

where $c = \sinh^{-1}(1) \approx 0.8814$ and $g(x)$ is given by

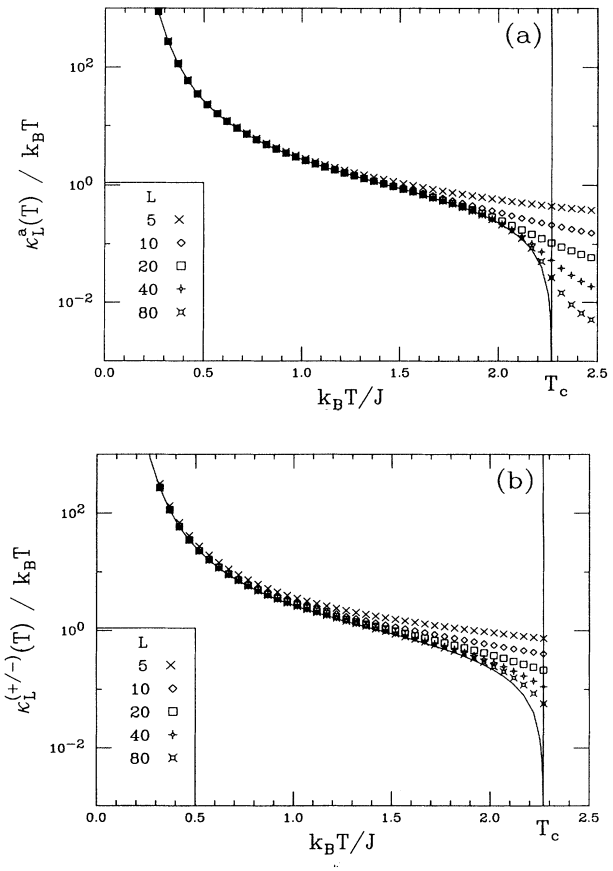

FIG. 5. The estimates of the surface stiffness coefficient in two dimensions. (a) $\kappa_L^a(T)$, from Eq. (18), and (b) $\kappa_L^{(+/-)}(T)$, from Eq. (24). The solid curve is the limit of $\kappa_L(T)$ for an infinite lattice (Ref. 34). The solid vertical line is the 2D critical temperature.

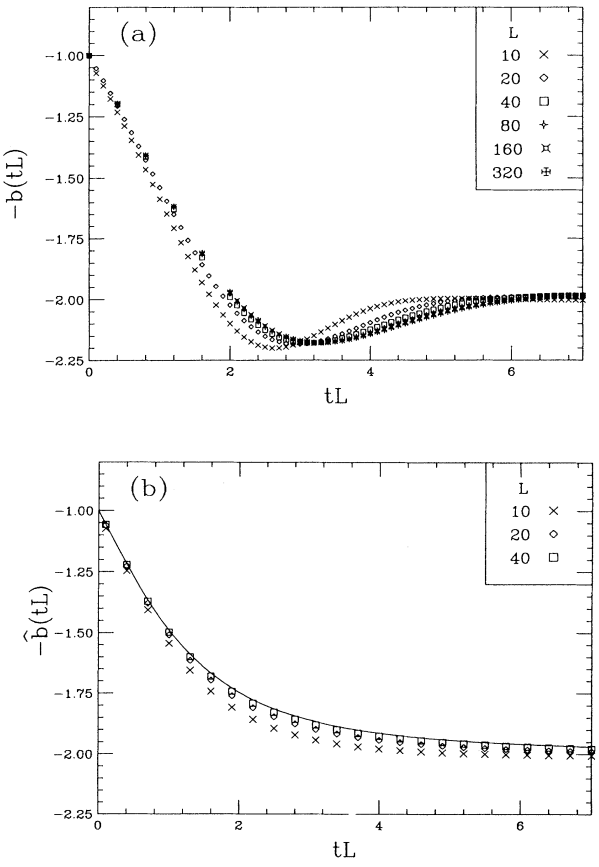

FIG. 6. The effective scaling exponents for the surface stiffness coefficient in two dimensions. (a) The scaling exponent $b(tL)$, defined in Eq. (20), for $\kappa_L^a(T)$. (b) The scaling exponent $\hat{b}(tL)$, defined in Eq. (B3), for $\hat{\kappa}_L(T)$. The solid curve is the limit for large L referenced in Eq. (22a) and derived in Appendix B.

$$g(x) = \sqrt{(2c)^2 + \left(\frac{\pi}{x}\right)^2} \ . \tag{22b}$$

Equation (22a) is derived in Appendix B. As is the case for $B(tL)$ and $b(tL)$, $\hat{b}(tL)$ varies from 1 at $tL=0$ to 2 at $tL=\infty$, but unlike $b(tL)$, $\hat{b}(tL)$ is monotonic [Fig. 6(b)]. It is proved in Appendix B that $\lim_{tL\to\infty} \hat{b}(tL) = 2$, and, since $\lim_{tL\to\infty} \hat{b}(tL) = \lim_{tL\to\infty} b(tL)$, we also have $\lim_{tL\to\infty} b(tL) = 2$.

Another capillary-wave calculation[21,22] indicates that for plus/minus boundary conditions the correlation length scales as

$$\xi_L^{(+/-)}(T) \approx \frac{2}{3\pi^2}\frac{\kappa(T)}{k_B T}(L+2)^2 \tag{23}$$

for all $T < T_c$, giving the finite-size estimate for the surface stiffness coefficient

$$\kappa_L^{(+/-)}(T) = k_B T \frac{3\pi^2}{2}\frac{\xi_L^{(+/-)}(T)}{(L+2)^2} \ . \tag{24}$$

Figure 5(b) shows $\kappa_L^{(+/-)}(T)$. We have observed numerically that for any fixed temperature $T \le T_c$, $\kappa_L^{(+/-)}(T)$ converges to $\kappa(T)$ as L^{-1}.[57]

B. κ in three dimensions

There are two contributions to the correlation length along the interface. The first comes from pieces of interface which, due to thermal fluctuations, are normal to the longitudinal direction, which is the direction in which the correlation length is measured. This contribution is related to the surface stiffness $\kappa(T)$. The second contribution comes from the formation of bubbles in the bulk and is much less important for $T \ll T_c$.

Both of these contributions can be treated approximately by considering a cross section of the 3D system parallel to the xy plane. The relationship between correlation length and surface stiffness in such a cross section should be the same as for a 2D system of the same width L. Since there are M such cross sections, and since each contributes on average the same amount of interface normal to the longitudinal direction, the total effective surface stiffness for the 3D system is given by $M\kappa(T)$ and has the same form as the corresponding 2D systems; that is, the appropriate estimate for the 3D surface stiffness coefficient for antiperiodic boundary conditions is given from Eq. (18) by

$$\kappa_{L,M}^{a}(T) = k_B T \frac{\pi^2}{2}\frac{\xi_{L,M}^{a}(T)}{L^2 M} \ , \tag{25}$$

and for plus/minus boundary conditions from Eq. (24) by

$$\kappa_{L,M}^{(+/-)}(T) = k_B T \frac{3\pi^2}{2}\frac{\xi_{L,M}^{(+/-)}(T)}{(L+2)^2 M} \ , \tag{26}$$

for $L \approx M \gg 1$. These estimates were proposed by Privman and Švrakić.[21,22] No part of this argument depends on the boundary conditions in the z direction, so Eqs. (25) and (26) are valid for either periodic or free boundary conditions applied in the z direction. In this article we discuss $\kappa(T)$ only in the case of periodic boundary conditions in the z direction, but we have observed that little quantitative change occurs when free boundary conditions are used.

In Fig. 7(a) the reduced correlation length, defined in 3D by analogy with Eq. (21), is used in place of $\xi_{L,M}^{a}(T)$ to estimate $\kappa(T)$ using Eq. (25). As in Sec. IV A, this produces a reduction in the estimate of $\kappa(T)$ near T_c [where $\kappa(T)$ is zero in an infinite system] but cannot have any effect on the estimate of $\kappa(T)$ for $T < T_c$ in the limit of large systems. Also shown in Fig. 7(a) are estimates of $\kappa(T)$ based on series expansions improved by Padé approximants[50] and estimates based on Monte Carlo simulations.[27] In spite of the small systems to which our study was limited, we find good agreement between the transfer-matrix estimates in this study and

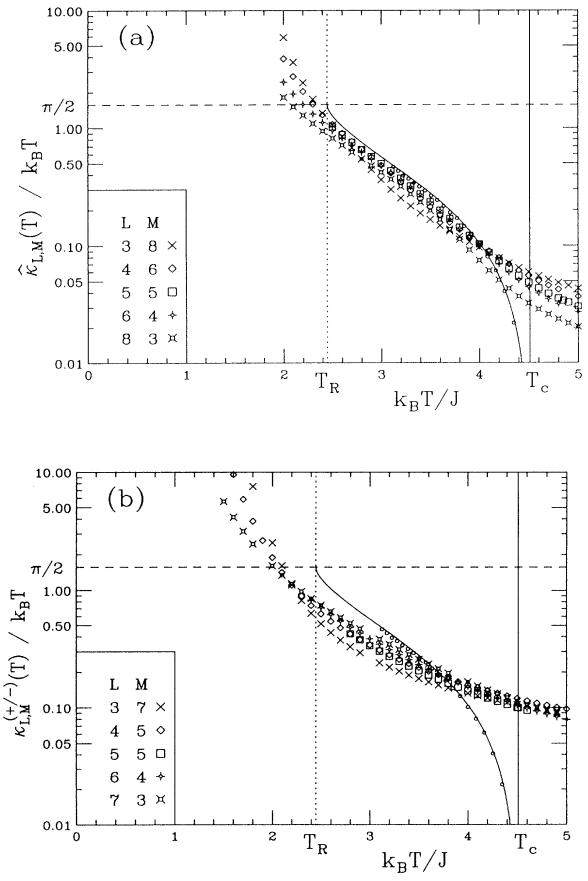

FIG. 7. The estimates of the surface stiffness coefficient in three dimensions. (a) $\hat{\kappa}_{L,M}(T)$, from Eq. (25), and (b) $\kappa_{L,M}^{(+/-)}(T)$, from Eq. (26). The solid curve comes from series expansions improved with Padé approximants (Ref. 50). The small solid circles (bigger than the error bars) are the results of Monte Carlo simulations (Ref. 27). The vertical dotted line indicates the roughening temperature, T_R, as determined from Monte Carlo studies (Ref. 3). The vertical solid line is the 3D critical temperature (Ref. 5).

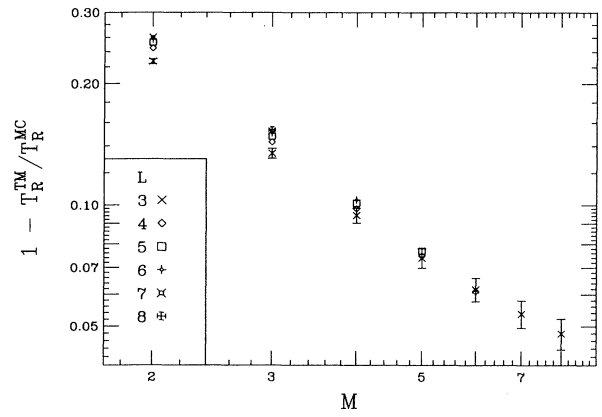

FIG. 8. The fractional difference between the transfer-matrix roughening temperature, T_R^{TM}, as determined from $\hat{\kappa}_{L,M}(T)/k_BT_R = \pi/2$, and the roughening temperature found from Monte Carlo simulations (Ref. 3), T_R^{MC}. The error bars (shown only for $L=3$) result from uncertainty in T_R^{MC}.

the previous estimates[27,50] over a wide range of temperatures between T_R and T_c.

In Fig. 7(b) we show the estimate for $\kappa(T)$ that results from using Eq. (26). Comparison with the series expansion and Monte Carlo estimates shows that finite-size corrections to Eq. (26) cannot be neglected at any temperature for the systems we studied.

The surface stiffness coefficient for the infinite system shows a characteristic KT discontinuity[7,8] at T_R, jumping from $\kappa(T) = \infty$ for all $T < T_R$ to $\kappa(T)/k_BT = \pi/2$ for $T = T_R^+$.[58] If we use the criterion $\kappa(T_R)/k_BT_R = \pi/2$ to estimate T_R while using antiperiodic boundary conditions, we find that the estimated value of T_R depends most strongly on the value of M (Fig. 8). For the system $(L, M) = (3, 8)$, we find $T_R \approx 2.337J/k_B$. This represents a deviation of approximately 5% from the Monte Carlo estimates,[3–5] and is comparable with our alternative estimates of T_R discussed in Sec. VI. Although the convergence in Fig. 8 appears to be roughly power law in behavior, much slower convergence should be expected for large systems due to the KT nature of the roughening transition.[59]

V. THE STEP FREE ENERGY

For $T < T_R$, a SOS calculation indicates that the correlation length for antiperiodic boundary conditions should scale as[21,22]

$$\xi^a_{L,M}(T) \approx \mu(T) M^w \exp\left[\frac{Ms(T)}{k_BT}\right] \left(\sin\frac{\pi}{2L}\right)^{-2}, \qquad (27)$$

where $\mu(T) \equiv \frac{1}{4}\exp[wC(T, L/M)]$, and $C(T, L/M)$ is a function possibly of the temperature, boundary conditions, and shape of the layer, but is independent of the size of the layer. The boundary conditions in the z direction may be either periodic [Fig. 9(a)] or free [Fig. 9(b)]. By taking three different values of M we can solve simultaneously for $s(T)$, $w(T)$, and $\mu(T)$. The step free energy $s(T)$ discussed in this article is the step free energy for an interface parallel to the xz plane. A low-temperature expansion for the step free energy of inclined planes can be found in Ref. 15.

Unfortunately, numerical convergence difficulties limit to very small systems our studies of interfaces at very low temperatures. Furthermore, quantities near T_R, where we can use larger systems, may be expected to be difficult to estimate due to the KT transition. Nevertheless, the estimates of $s(T)$ rapidly converge at low temperatures, so that the limitation to small systems may not present difficulties in estimating the step free energy. Also, the estimates of $s(T)$ are rather insensitive to the values of w and $\mu(T)$, so that problems at low temperatures with the last two quantities (described below) do not seem to create difficulties in the estimates of $s(T)$. This is because the divergence of the correlation length at low tempera-

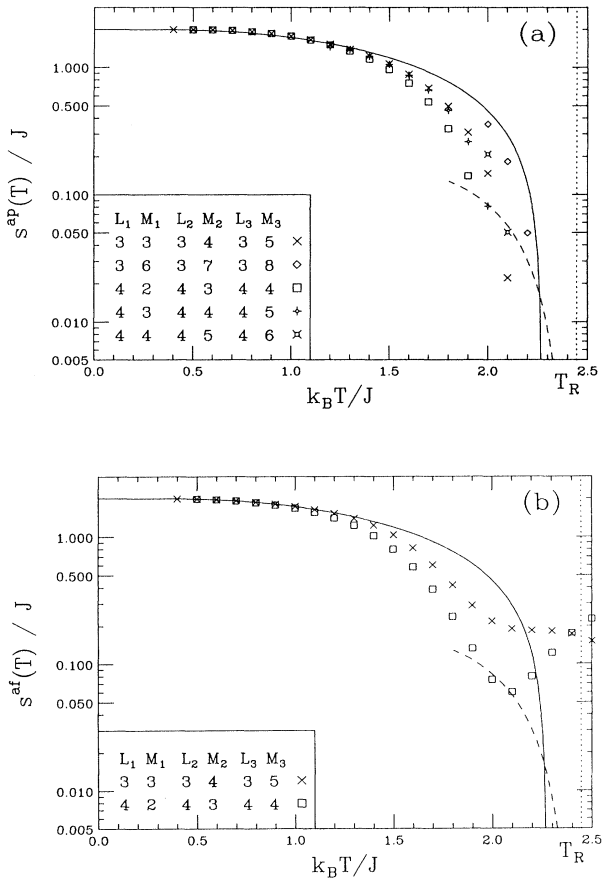

FIG. 9. The estimates for the step-free energy using antiperiodic boundary conditions in the y direction. Estimates using periodic and free boundary conditions in the z direction are given by (a) $s^{\mathrm{ap}}(T)$ and (b) $s^{\mathrm{af}}(T)$, respectively. By keeping the temperature constant and taking three different values of M (and any combination of values of L), we solve Eq. (27) simultaneously for s, w, and μ. The solid curve is the 2D surface free energy. The dashed curve shows the estimate Eq. (29) (Refs. 24 and 61).

tures is dominated by the exponential factor in Eq. (27), which contains the step free energy.

The estimates of $s(T)$ derived from Eq. (27) are compared in Fig. 9 with approximations valid either near $T=0$ or near $T=T_R$. At low temperatures the interface becomes a series of plateaus separated in height from their neighbors by one lattice spacing. These plateaus are equivalent to domains in a 2D system;[15,22] the equivalence is exact at $T=0$. This yields the well-known approximation[15]

$$s(T) \approx \tau^{2D}(T) . \tag{28}$$

We use $\tau^{2D}(T)$ as an approximation to $s(T)$ for $T \ll T_R$ for the following reasons: It provides a simple physical picture, it agrees with the first several terms of low-temperature series expansions of $s(T)$;[15] it has been solved exactly;[33] and the 2D critical temperature is a rigorous lower bound on T_R.[60] At higher temperatures ($T \approx T_R$), $s(T)$ shows the characteristic KT essential singularity at T_R,[6-8] and is given by

$$\frac{s(T)}{k_B T} \approx \exp\left(-\frac{\pi}{2c}\sqrt{\frac{T_c}{T_R - T}}\right) , \tag{29}$$

where the nonuniversal parameter c has been found by Monte Carlo simulations[24,61] to be $c = 1.57 \pm 0.07$. In Fig. 9 we have calculated the estimate Eq. (29) with $c = \pi/2$.

The correspondence between a low-temperature interface in 3D and a 2D system ensures[53,62-64] that for periodic boundary conditions in the z direction $w = 1/2$, whereas for free boundary conditions in the z direction $w=0$. Our estimates, however, have $w=0$ for sufficiently low temperatures for both sets of boundary conditions (Fig. 10). The incorrect estimate for w in the case of periodic boundary conditions in the z direction provides a caution that the asymptotic scaling regime, in which corrections to Eq. (27) can be expected to be very small, has not been reached with the current small systems. The parameter $\mu(T)$ (not shown) is consistent with $w=0$ at low temperatures.

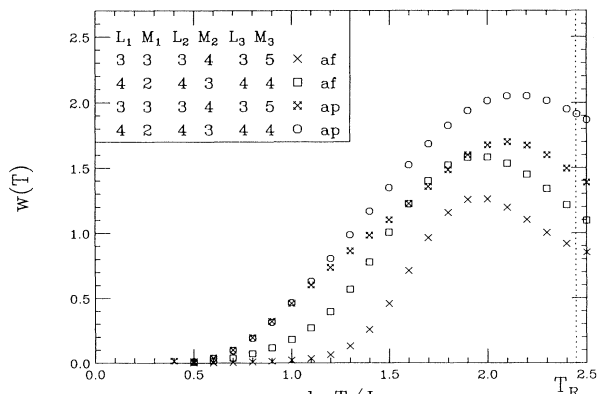

FIG. 10. The estimates for the exponent w, found by solving Eq. (27) for $s(T)$, w, and $\mu(T)$, where the boundary conditions in the y direction are antiperiodic. It is known that at $T=0$ $w=1/2$ for periodic boundary conditions (ap) in the z direction and that $w=0$ for free boundary conditions (af). At low temperatures our transfer-matrix estimates give that $w=0$ for both sets of boundary conditions, indicating the presence of substantial corrections to scaling.

For plus/minus boundary conditions, the scaling relation

$$\xi_{L,M}^{(+/-)}(T) \approx \mu(T) M^w \exp\left[\frac{M s(T)}{k_B T}\right] \times \left[\sin\frac{3\pi}{2(L+2)} \sin\frac{\pi}{2(L+2)}\right]^{-1} \tag{30}$$

is expected in analogy with Eq. (27) on the basis of another SOS calculation.[21,22] The analysis for Eq. (30) parallels that for Eq. (27), so that at zero temperature we should find that for periodic boundary conditions in the z direction $w=1/2$, and that for free boundary conditions $w=0$. In this case the values extracted for $s(T)$ (not shown) for different system sizes are inconsistent with each other even at low temperatures, and the corresponding values of w (also not shown) show no pattern whatsoever.

In short, the scaling relation of Eq. (27) yields values of the step free energy that are consistent with the low-temperature approximation $\tau^{2D}(T)$, whereas Eq. (30) does not even yield consistent estimates at low temperatures. The parameter $w(T)$ is found to be wrong at low temperatures when calculated from Eq. (27) with periodic boundary conditions in the z direction, and when calculated from Eq. (30) it yields inconsistent values. It is thus apparent that large corrections to scaling are present for the systems in this study.

VI. THE CALLAN-SYMANZIK β FUNCTION IN THE ROUGH PHASE

In Secs. IV B and V we have evaluated terms in the surface tension from FSS relations for the correlation length[21,22] in 3D for $0 < T < T_c$. As discussed in Sec. IV B, for $T_R \le T \le T_c$ each of the M cross-sections parallel with the xy plane makes a contribution to the correlation length in an $\infty \times L \times M$ system, which is of the same form as the correlation length in a 2D system of width L. From this argument we have Eqs. (25) and (26), which give $\xi_{L,M} \propto M$ for either antiperiodic or plus/minus boundary conditions. Such linear divergence with system size of the correlation length is characteristic of a critical point,[31] and indicates that the rough phase of the interface is a critical phase.[1] A quantity that has proven particularly useful in locating such extended critical phases in previous studies (e.g., Refs. 65 and 66) of systems with KT behavior is the Roomany-Wyld approximant to the Callan-Symanzik β function.[40,41] This approximant is defined by

$$\beta_{L,M}(T) = \frac{(d\ln[\xi_{L,M}/L^2])/(d\ln M) - 1}{(d\ln[\xi_{L,M}/L^2])/(dT)} , \tag{31}$$

where the derivative with respect to $\ln M$ is evaluated by multiple-point finite differences. [There should be

no confusion between $\beta_{L,M}(T)$ and the dimensionless inverse temperature, which is called β in the appendixes.] Within the region where a "critical interface" exists, one should have $\beta_{L,M}(T) = \text{const} \approx 0$. In this section we apply the β function to the 3D Ising model with antiperiodic boundary conditions in order to obtain independent TM FSS estimates both for T_R and for the (size-dependent) temperature where the rough-interface phase is destroyed by critical-point fluctuations in the small systems we are studying.

In Fig. 11 we show various estimates of $\beta_{L,M}(T)$ for the case of antiperiodic boundary conditions in the y direction and periodic boundary conditions in the z direction. Finite-size effects were larger for the case of free boundary conditions in the z direction and much larger for the case of plus/minus boundary conditions in the y direction, so these results are not shown. The dashed curve near $T = 0$ is the value of $\lim_{L,M\to\infty} \beta_{L,M}(T)$, where $\tau^{2D}(T)$ is substituted for $s(T)$ in Eq. (27). If the scaling relations of Eqs. (27) and (30) for $T < T_R$ are to join continuously with the scaling relations of Eqs. (25) and (26) for $T > T_R$ at T_R, then $w(T_R) = 1$. The solid curve for $T \le T_R$ traces $\lim_{L,M\to\infty} \beta_{L,M}(T)$ under the assumptions that Eq. (27) holds near T_R with $w = 1$, and that the step-free energy near T_R is given by Eq. (29). The agreement of the data in Fig. 11 with this portion of the solid curve is good despite the fact that Eq. (27) is based on the assumption that the terraces in the interface are well separated, which is not the case near T_R. The solid horizontal line $\beta_{L,M}(T) = 0$ for the temperature range $T_R \le T \le T_c$ shows $\lim_{L,M\to\infty} \beta_{L,M}(T)$ assuming that Eq. (25) holds in this range.

The finite-size estimates for $\beta_{L,M}(T)$ are of two types. The first type consists of evaluating $(d\ln[\xi_{L,M}/L^2])/(d\ln M)$ by a three-point estimate while holding L constant, and then making the empirical extrapolation

$$\beta_{L,(M\to\infty)}(T) = \beta_{L,M}(T) + a(T)\exp[-b(T)M], \tag{32}$$

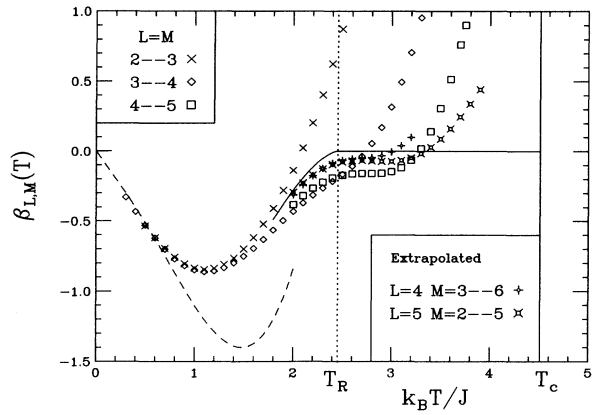

FIG. 11. Finite-size estimates for the Callan-Symanzik β function, given in Eq. (31). Results are shown both for sets of systems with square cross sections and for extrapolations based on Eq. (32). The solid curve comes from inserting the estimate of Eq. (29) (Ref. 61) for $s(T)$ for $T \approx T_R$ into Eq. (27). The dashed curve comes from an approximation of the step-free energy by the 2D surface-free energy in Eq. (27).

where $a(T)$ and $b(T)$ are unknowns that depend only on temperature. (The only justification for this extrapolation procedure is that it appears to work nicely for small systems, although we expect logarithmic convergence for large systems because roughening is a KT transition.[59]) For $L > 3$ this yields results which depend little on M and show the emergence of a plateau near T_R with $\beta_{L,M}(T) \approx -0.06$. Even for $L = 5$, critical finite-L effects destroy the plateau for temperatures greater than about $3.2J/k_B$. The extrapolated value of $\beta_{L,(M\to\infty)}(T)$ for $L = 3$ does not show any plateau, but there is a change in concavity at about $2.41J/k_B$, where the critical finite-L effect gives way to the $T < T_R$ behavior.

The second type of finite-size estimate is made by using only systems with square cross sections ($L = M$) in the numerical evaluation of $(d\ln[\xi_{L,M}/L^2])/(d\ln M)$ in Eq. (31). For the largest such pair of systems, this estimate of $\beta_{L,M}(T)$ yields a plateau at $\beta_{L,M}(T) \approx -0.2$.

In either case, the onset of the plateau (which corresponds to an estimate of T_R) can be defined by a peak in $d^2\beta_{L,M}(T)/dT^2$. This estimate yields $T_R \approx 2.3J/k_B$, which is approximately the same as that found in Sec. IV B. The high-temperature end of the plateau seems to correspond to the temperature at which critical finite-L effects become large in the interface internal energy (not shown), which is given by

$$U = -T^2 \frac{\partial(\tau/T)}{\partial T} . \tag{33}$$

VII. DISCUSSION AND CONCLUSION

As a nonperturbative numerical method for studying semi-infinite systems in equilibrium, numerical transfer-matrix (TM) calculations followed by finite-size scaling[21,22] (FSS) provide an appealing alternative to the analytical and Monte Carlo methods which have been used to study interfaces in the Ising model. Nevertheless, the rapid growth of the order of the transfer matrix with system size has limited most previous studies to solid-on-solid (SOS) and capillary-wave approximations.

In this paper we have performed large-scale numerical TM calculations on a Cray Y-MP/432 and a Thinking Machines Corporation CM2 to obtain the correlation lengths and free energies of 2D and 3D Ising ferromagnets with interfaces, which are related to the surface tension anisotropy through the scaling relations derived in Refs. 21 and 22. In 2D we are able to analyze the corrections to scaling. In 3D we are only able to confirm the scaling relations for antiperiodic boundary conditions, and the resulting estimates for $\tau(T)$ and $\kappa(T)$ agree well with estimates from series expansions improved with Padé approximants[50] and from Monte Carlo simulations.[27] For plus/minus boundary conditions the finite-size effects in our estimates are still large, even for the largest systems which can be studied using current supercomputers and algorithms, and the asymptotic scaling regime has not been reached.

We find that although in 2D the surface free energy converges exponentially for antiperiodic boundary conditions, for plus/minus boundary conditions the conver-

gence obeys a power law. The effective scaling exponent for plus/minus boundary conditions is a function only of the critical scaling variable tL, and varies monotonically from 1 at $tL = 0$ to 2 as $tL \to \infty$. Although the exact value of $\tau(T)$ is not known in 3D for arbitrary temperatures, our numerical results for $L = M$ agree well with the estimates of Refs. 27 and 50. In 3D we are not able to make a quantitative study of the scaling.

In 2D the surface stiffness coefficient is found from scaling relations based on capillary-wave studies.[21,22] For antiperiodic boundary conditions we find that $\kappa_L^a(T)$ at any fixed temperature $T < T_c$ converges in a power-law fashion with an effective exponent similar to that found for $\tau^{(+/-)}(T)$. Specifically, for large L the exponent is a function only of the critical scaling variable tL, and varies from 1 at $tL = 0$ to 2 as $tL \to \infty$, though not monotonically. By using the "reduced" correlation length, a monotonic exponent, discussed in Appendix B, can be calculated in the infinite-lattice limit. For plus/minus boundary conditions $\kappa_L^{(+/-)}(T)$ converges simply as $1/L$.

The estimates for $\kappa(T)$ in 3D are based on scaling relations similar to those in 2D because of the similarity of a cross section in 3D to a 2D system. These estimates[21,22] in the case of antiperiodic boundary conditions agree well with both series[50] and Monte Carlo[27] estimates. Plus/minus boundary conditions lead to large finite-size effects in the estimates of $\kappa(T)$ at all temperatures. Estimates for the roughening temperature based on the KT relation $\kappa(T_R)/k_B T_R^+ = \pi/2$ (Refs. 7, 8, and 58) depend more strongly on the value of M than on the value of L. For $(L, M) = (3, 8)$, this estimate yields $T_R \approx 2.3$.

Solid-on-solid arguments have yielded scaling relations for the correlation length,[21,22] which we exploit to find $s(T)$. In the case of antiperiodic boundary conditions, the estimates for $s(T)$ agree well with other approximations at low temperatures. The low-temperature value of the fitting parameter w of Eq. (27) for systems with periodic boundary conditions in the z direction, however, is in contradiction with known results.[53,62–64] This indicates the presence of corrections to scaling for the correlation length in the small systems of this study. These corrections are even more pronounced in the case of plus/minus boundary conditions, where the values of $s(T)$ estimated from different system sizes are inconsistent even at low temperatures.

The rough phase of the interface, which is a type of critical phase,[1] displays scaling behavior for the correlation length, which is similar to that of other critical systems.[31] Specifically, as a result of Eq. (25), we have $\xi \propto M$. We used the Roomany-Wyld approximant to search for a plateau in the Callan-Symanzik β function,[40,41] which corresponds to this critical temperature range. The onset of the plateau agrees roughly with the estimate of T_R from Sec. IV B, while the end of the plateau corresponds to the onset of large-scale finite-size corrections in the interface internal energy caused by the disappearance of the interface at T_c.

In summary, we have provided transfer-matrix finite-size scaling estimates of the quantities which characterize the surface-tension anisotropy in two- and three-dimensional Ising ferromagnets: the surface free energy $\tau(T)$, the surface stiffness coefficient $\kappa(T)$, and the step free energy $s(T)$. Our results support the analytically obtained relations of Refs. 21 and 22 and are fully consistent with existing series and Monte Carlo estimates.[27,50] However, we find that in the three-dimensional case the limitations of current computer technology and algorithms do not permit transfer-matrix studies of sufficiently large systems to improve on the numerical accuracy of the previously existing estimates.

ACKNOWLEDGMENTS

The authors wish to thank K. K. Mon and V. Privman for useful discussions, M. Grant for a reading of the manuscript, and P. E. Oppenheimer for discussions about PARIS programming of the CM-2. The authors would also like to thank M. E. Fisher for assistance in locating relevant research and for providing unpublished independent series estimates from his work with H. Wen. The authors wish to thank M. Hasenbusch and K. Pinn for providing unpublished independent Monte Carlo estimates for comparison, and M. Hasenbusch for helpful comments on an earlier version of this paper. This research was supported in part by the Florida State University Supercomputer Computations Research Institute, which is partially funded by the U.S. Department of Energy through Contract No. DE-FC05-85ER25000, by the FSU Center for Materials Research and Technology, and by the National Science Foundation through Grant No. DMR-9013107.

APPENDIX A: COMPUTATIONAL DETAILS

This appendix contains details about the algorithms used in the diagonalization and the programming implementation of these algorithms. In this appendix we take $k_B = J = 1$, so that all quantities are dimensionless.

If each of the identical layers has A spin sites, the $2^A \times 2^A$ transfer matrix $\underline{T}$ in Eq. (6) can be decomposed into the product of two matrices, $\underline{T} = \underline{A}\underline{D}$. The matrix $\underline{D}$, which can be chosen to be diagonal, takes into account both interactions between spins in the same layer and interactions of the spins with a magnetic field. The matrix $\underline{A}$ takes into account the interaction between one layer and the next layer in the manner of the third line of Eq. (6). It is a direct (Kronecker) product of A identical 2×2 matrices

$$\underline{a} = \begin{pmatrix} e^{\beta} & e^{-\beta} \\ e^{-\beta} & e^{\beta} \end{pmatrix}, \tag{A1}$$

where $\beta = 1/T$. In both of the algorithms used, as described below, the core of the algorithm demands that for any given vector $\mathbf{v}$ one can obtain a vector $\mathbf{w} = \underline{T}\mathbf{v}$. In order to be able to find even a few of the largest eigenvalues of $\underline{T}$ with A large, one needs to minimize the computer storage required. This means that only a few (typically between 2 and 20) vectors of size 2^A can be stored, whereas the entire 2^{2A} elements of $\underline{T}$ cannot be stored. The matrix $\underline{D}$ only requires storage of 2^A elements, so it

is computed once for each temperature and stored. All of the boundary conditions used in this paper are incorporated into the matrix $\underline{D}$. Two slightly different methods of computing $\underline{A}\mathbf{x}$ were used.

Although the size of the matrix $\underline{T}$ can be reduced by consideration of the symmetries of the model, the savings in computer storage are not great in systems into which an interface, which breaks many symmetries, has been introduced. Furthermore, the symmetry-reduced matrix would reduce the speed of the diagonalization program discussed below on the CM-2 by complicating interprocessor communications. Since very few systems with reasonable aspect ratios could be added by using symmetry reduction, and because it would be inefficient to implement symmetry reduction on the systems now accessible, we have not pursued this.

For $A \leq 19$, the Numerical Algorithms Group (NAG) routine F02FJE was used on the Florida State University Cray Y-MP computer, which has 32 MWords of memory. This routine required use of the symmetric transfer matrix $\underline{D}^{1/2}\underline{A}\underline{D}^{1/2}$. One can write $\underline{A} = \underline{A}_A\underline{A}_{A-1}\cdots\underline{A}_1$, where each $2^A \times 2^A$ matrix $\underline{A}_i$ is a direct product of $A-1$ identity matrices of size 2×2 and the matrix $\underline{a}$ in position i. A permutation matrix $\underline{P}$ can be defined such that $\underline{P}^{-1}\underline{A}_i\,\underline{P} = \underline{A}_{i+1}$ with $\underline{A}_{A+1} = \underline{A}_1$. In other words, $\underline{P}$ permutes the matrices within the Kronecker product in a cyclic fashion.[67–72] For any j, it follows that $\underline{A}_j = \underline{P}^{-j+1}\underline{A}_1\underline{P}^{j-1}$, and thus one obtains $\underline{A} = \underline{P}^{-A+1}\underline{A}_1(\underline{P}\underline{A}_1)^{A-1}$. Since $\underline{P}^{-A}$ is the identity matrix, all one needs to do is to program the multiplication of a vector by $\underline{A}_1$ and by $\underline{P}$ and repeat these A times to obtain the multiplication by $\underline{A}$. The matrix $\underline{A}_1$ has only two nonzero elements in each row and column, so multiplication by $\underline{A}_1$ can be efficiently programmed. One way of doing this is to break the vector to be multiplied into an upper and a lower part, each having 2^{A-1} elements. Then

$$\underline{A}_1\begin{pmatrix}\mathbf{v}_a\\ \mathbf{v}_b\end{pmatrix} = e^{\beta}\begin{pmatrix}\mathbf{v}_a\\ \mathbf{v}_b\end{pmatrix} + e^{-\beta}\begin{pmatrix}\mathbf{v}_b\\ \mathbf{v}_a\end{pmatrix}. \tag{A2}$$

The matrix $\underline{P}$ acts on a vector as $\underline{P}\binom{\mathbf{v}_a}{\mathbf{v}_b} = \mathbf{w}$, with the ith even element of $\mathbf{w}$ given by the ith element of $\mathbf{v}_b$ and the ith odd element of $\mathbf{w}$ given by the ith element of $\mathbf{v}_a$. The multiplication by $\underline{P}$ can be efficiently programmed using scatter-gather routines on a vector computer.

For $14 \leq A \leq 25$, a double-precision program in FORTRAN/PARIS for a Thinking Machines Corporation massively parallel CM-2 computer was used for the diagonalization. The use of the PARIS programming language was essential for diagonalization of the large matrices, since the FORTRAN compiler would have otherwise allocated more than the minimum number of arrays. Programming simplicity in the PARIS portion of the program required that the number of 1-bit processors used be less than or equal to the size of a single vector. The CM-2 available has 2^{16} processors, and can be divided into quarters with 2^{14} processors each, giving the limit $14 \leq A$. The upper limit was imposed by the computer memory on the CM-2. To calculate the correlation length, at least two vectors need to be iterated. This entailed storing six double-precision (64-bit) vectors: One of these was a work vector, one was the vector associated with the diagonal matrix $\underline{D}$, and two vectors each were for the current iteration vector and for the next iteration vector. In addition, $A-1$ single-bit vectors were used to efficiently implement the multiplication of a vector by the matrices $\underline{A}_i$. (Temporary vectors used in the formation of the bit vectors and of the diagonal matrix were discarded before the 64-bit iteration vectors were allocated.) For $A = 25$, this required use of 1.7 Gbytes of the available 2 Gbytes of main memory on the CM-2. The implementation of the multiplication by one of the A matrices $\underline{A}_i$ was made using the hypercube communication of the CM-2 computer. This was done by using the decomposition $\underline{A}_i = e^{\beta}\underline{I} + e^{-\beta}\underline{X}_i$. Here $\underline{I}$ is the $2^A\times 2^A$ identity matrix, and the permutation matrix $\underline{X}_i$ is a direct product of A–1 identity matrices of size 2×2 and the matrix $\underline{X} = \left(\begin{smallmatrix}0&1\\1&0\end{smallmatrix}\right)$ in the ith position. The multiplication by the $\underline{X}_i$ matrices was performed using efficient communication with the PARIS command GET_FROM_POWER_TWO, which allows hypercube communication to elements a power of two away.

The program was written to diagonalize any real matrix with both the largest eigenvalues and corresponding eigenvectors real. The algorithm used is based on a generalized power method and proceeds as follows.[73] A $2^A\times R$ matrix $\underline{U}$ is initialized with random elements. Due to constraints of the PARIS program, R must be an integer power of 2, and memory constraints dictate that $R=2$ if $A=25$. Then the $2^A\times R$ matrix $\underline{V} = \underline{T}\,\underline{U}$ is obtained using the multiplication procedure described above for each of the R vectors in $\underline{V}$. Two $R\times R$ matrices $\underline{\mathcal{S}} = \underline{U}^T\underline{U}$ and $\underline{\mathcal{Q}} = \underline{U}^T\underline{V}$ are then formed. The eigenvalue equation $\underline{\mathcal{S}}^{-1}\underline{\mathcal{Q}}\,\underline{\mathcal{G}} = \underline{\mathcal{G}}\,\underline{\mathcal{D}}$ is then solved to find the $R\times R$ diagonal matrix of eigenvalues $\underline{\mathcal{D}}$ and the $R\times R$ orthogonal matrix of normalized eigenvectors $\underline{\mathcal{G}}$. The diagonal elements of $\underline{\mathcal{D}}$ provide the estimates for the eigenvalues of the transfer matrix $\underline{T}$ for this iteration. The matrix $\underline{U}$ is then updated by $\underline{U} \leftarrow \underline{V}\,\underline{\mathcal{G}}$, and the process is repeated.

Near T_c typically about 25 iterations were necessary to obtain convergence of the correlation length to one part in 10^{15}. However, at lower temperatures many more iterations were required for convergence. Near T_c for $A = 25$, the computer time required for convergence on the 2^{16} processor CM-2 with double-precision Weitek floating-point accelerators was about 15 min.

APPENDIX B: THE SCALING EXPONENT FOR $\hat{\kappa}$ IN 2D

In Eq. (22a) in Sec. IV A we presented the exact result for an effective scaling exponent $\hat{b}(L,T)$ such that

$$\hat{\kappa}_L(T) - \kappa(T) \approx \hat{a}L^{-\hat{b}}. \tag{B1}$$

In analogy with Eq. (20),

$$\hat{b}(L,T) \equiv \frac{d\ln[\hat{\kappa}_L(T)-\kappa(T)]}{d\ln L} \tag{B2}$$

$$= -\frac{L}{\hat{\kappa}_L(T)-\kappa(T)}\frac{d\hat{\kappa}_L(T)}{dL}. \tag{B3}$$

This appendix contains a sketch of a derivation of Eq. (22a), which is made by rewriting the functions in Eq. (B3) in terms of the reduced temperature $t \equiv (T_c - T)/T_c$ and the critical scaling variable $x = tL$, and then keeping only the $O(1)$ term in t at fixed x. In this appendix we take $k_B = J = 1$ and measure the surface stiffness coefficient in units of $k_B T$, so that all quantities are dimensionless.

First, we define the functions which are to be expanded. These are[21,22,34] the inverse temperature

$$\beta = 1/T \ , \tag{B4}$$

the Onsager angles

$$\gamma(0) = 2\beta + \ln[\tanh(\beta)] \tag{B5a}$$

and

$$\gamma(\pi/L) = \cosh^{-1}[A - \cos(\pi/L)] \ , \tag{B5b}$$

where

$$A \equiv \frac{\cosh^2(2\beta)}{\sinh(2\beta)} \ , \tag{B6}$$

the "reduced" mass gap, which is the sum of the mass gaps for antiperiodic and periodic boundary conditions,

$$\begin{aligned} \hat{m}_L(T) &= [\hat{\xi}_L(T)]^{-1} \equiv [\xi_L^a(T)]^{-1} + [\xi_L^p(T)]^{-1} \\ &= \gamma(\pi/L) - \gamma(0) \ , \end{aligned} \tag{B7}$$

the reduced surface stiffness coefficient

$$\hat{\kappa}_L(T) = \frac{\pi^2}{2L^2 \hat{m}_L} \ , \tag{B8}$$

and the surface stiffness coefficient in the limit $L \to \infty$

$$\kappa = \sinh \gamma(0) \ . \tag{B9}$$

Note that although L was initially allowed to take only integer values in Eqs. (B5b)–(B8), we drop this constraint to find a function $\hat{\kappa}_L(T)$, which is smooth and differentiable with respect to L.

Inserting Eqs. (B4)–(B9) into Eq. (B3), we find

$$\begin{aligned} \frac{d\hat{\kappa}_L(T)}{dL} &= \frac{\pi^2}{2L^2 \hat{m}_L} \left\{ \frac{-2}{L} - \frac{1}{\hat{m}_L} \frac{d\hat{m}_L}{dL} \right\} \\ &= \hat{\kappa}_L \left\{ \frac{-2}{L} - \frac{1}{\hat{m}_L} \frac{d\gamma(\pi/L)}{dL} \right\} \\ &= \hat{\kappa}_L \left\{ \frac{-2}{L} + \frac{\pi}{L^2 \hat{m}_L} \frac{d\gamma(\pi/L)}{d(\pi/L)} \right\} \qquad \text{(B10a)} \\ &= -2\hat{\kappa}_L \left\{ \frac{1}{L} - \frac{\hat{\kappa}_L}{\pi} \frac{\sin(\pi/L)}{\sqrt{[A - \cos(\pi/L)]^2 - 1}} \right\} \ , \qquad \text{(B10b)} \end{aligned}$$

so that

$$\begin{aligned} \hat{b}(L,T) = \frac{2L\hat{\kappa}_L(T)}{\hat{\kappa}_L(T) - \kappa(T)} \\ \times \left\{ \frac{1}{L} - \frac{\hat{\kappa}_L}{\pi} \frac{\sin(\pi/L)}{\sqrt{[A - \cos(\pi/L)]^2 - 1}} \right\} . \end{aligned} \tag{B10c}$$

It is convenient to define

$$c \equiv \frac{2}{T_c} = \sinh^{-1}(1) \ . \tag{B11}$$

A little algebra then yields the Taylor expansion

$$A \approx 2 + 2c^2 t^2 \ . \tag{B12}$$

With this result, and with $L = x/t$, it is easy to find that

$$\begin{aligned} \cosh \gamma(\pi/L) &= A - \cos\left(\frac{\pi t}{x}\right) \\ &\approx (2 + 2c^2 t^2) - \left(1 - \frac{1}{2}\left[\frac{\pi t}{x}\right]^2\right) \\ &= 1 + \frac{1}{2} g^2(x) t^2 , \end{aligned} \tag{B13}$$

where for convenience we have defined

$$g(x) = \sqrt{(2c)^2 + \left(\frac{\pi}{x}\right)^2} \ . \tag{B14}$$

Now taking $\cosh^{-1}$ of Eq. (B13) gives

$$\begin{aligned} \gamma(\pi/L) &= \cosh^{-1}\left(A - \cos\left[\frac{\pi t}{x}\right]\right) \\ &\approx g(x) t \ . \end{aligned} \tag{B15}$$

We also expand $\gamma(0)$ in a Taylor series to give

$$\begin{aligned} \gamma(0) &= 2\beta + \ln(\tanh[\beta]) \\ &\approx \gamma(0)\Big|_{t=0} + t \frac{d\gamma(0)}{dt}\Big|_{t=0} \\ &= 0 + 2ct \ . \end{aligned} \tag{B16}$$

From Eq. (B9) this implies

$$\kappa \approx 2ct. \tag{B17}$$

Using Eqs. (B7), (B8), (B15), and (B16) provides

$$\begin{aligned} \hat{\kappa}_L &= \frac{\pi^2 t^2}{2x^2\{\gamma(\pi/L) - \gamma(0)\}} \\ &= \frac{\pi^2 t}{2x^2\{g(x) - 2c\}} \ . \end{aligned} \tag{B18}$$

In order to evaluate $\hat{b}(x)$ it is also necessary to utilize

$$\begin{aligned} \frac{d\gamma(\pi/L)}{d(\pi/L)} &= \frac{\sin(\pi/L)}{\sqrt{[A - \cos(\pi/L)]^2 - 1}} \\ &\approx \frac{(\pi t/x)}{\sqrt{\left[1 + \frac{1}{2} g^2(x) t^2\right]^2 - 1}} \\ &\approx \frac{\pi}{x g(x)} . \end{aligned} \tag{B19}$$

Then, using Eq. (B10a)

$$\begin{aligned} \frac{d\hat{\kappa}_L}{dL} &= \hat{\kappa}_L \left\{ \frac{-2}{L} + \frac{\pi}{L^2 \hat{m}} \frac{d\gamma(\pi/L)}{d(\pi/L)} \right\} \\ &\approx \frac{\pi^2 t}{2x^2[g(x) - 2c]} \left\{ \frac{-2t}{x} + \frac{2}{\pi} \hat{\kappa}_L \frac{\pi}{x g(x)} \right\} . \end{aligned} \tag{B20}$$

Using this and Eq. (B18) we find

$$L\frac{d\hat{\kappa}_L}{dL} \approx L\frac{\pi^2 t}{2x^2[g(x)-2c]}\left\{\frac{-2t}{x}+\frac{2\hat{\kappa}_L}{xg(x)}\right\}$$
$$\approx -2\left\{\frac{\pi^2 t}{2x^2[g(x)-2c]}\right\}$$
$$\times\left\{1-\frac{\pi^2}{2x^2 g(x)[g(x)-2c]}\right\}. \quad \text{(B21)}$$

Finally we can combine Eqs. (B3), (B17), (B18), and (B21) to obtain

$$\hat{b}(x) = -\frac{L}{\hat{\kappa}_L(T)-\kappa(T)}\frac{d\hat{\kappa}_L(T)}{dL}$$
$$\approx 2\left(\frac{\pi^2 t/2x^2[g(x)-2c]}{\{\pi^2 t/2x^2[g(x)-2c]\}-2ct}\right)$$
$$\times\left(1-\frac{\pi^2}{2x^2 g(x)[g(x)-2c]}\right)$$
$$= 2\left(\frac{1}{1-4cx^2[g(x)-2c]/\pi^2}\right)$$
$$\times\left(1-\frac{\pi^2}{2x^2 g(x)[g(x)-2c]}\right), \quad \text{(B22)}$$

which is correct to $O(1)$ in t. Since we are interested in $\hat{b}(x)$ in the limit $t \to 0$ (which for fixed x necessarily means $L \to \infty$), this is the final answer.

It is instructive to determine $\hat{b}(x)$ for $x = 0$ and $x \to \infty$. Since we can write

$$xg(x) = \sqrt{(2cx)^2+\pi^2}\,, \quad \text{(B23)}$$

we immediately find

$$\lim_{x\to 0} xg(x) = \pi. \quad \text{(B24)}$$

Substituting this into Eq. (B22), we find

$$\hat{b}(x=0) = 1, \quad \text{(B25)}$$

which agrees with critical scaling.[31] We also note that

$$\lim_{x\to\infty} x^2[g(x)-2c] = \lim_{x\to\infty} c\left(\frac{\pi}{2c}\right)^2\left[1-\frac{1}{4}\left(\frac{\pi}{2cx}\right)^2\right], \quad \text{(B26)}$$

so that Eq. (B22) yields

$$\lim_{x\to\infty}\hat{b}(x) = 2. \quad \text{(B27)}$$

[1] H. van Beijeren and I. Nolden, in *Structure and Dynamics in Interfaces II*, Topics in Current Physics, Vol. 43, edited by W. Schommers and P. van Blanckenhagen (Springer-Verlag, Berlin, 1987).
[2] S. T. Chui and J. D. Weeks, Phys. Rev. B **14**, 4978 (1976).
[3] M. Hasenbusch, Ph.D. thesis, Universität Kaiserslautern, 1992.
[4] K. K. Mon, D. P. Landau, and D. Stauffer, Phys. Rev. B **42**, 545 (1990).
[5] C. F. Baillie, R. Gupta, K. A. Hawick, and G. S. Pawley, Phys. Rev. B **45**, 10 438 (1992).
[6] H. van Beijeren, Phys. Rev. Lett. **38**, 993 (1977).
[7] J. M. Kosterlitz and D. J. Thouless, J. Phys. C **6**, 1181 (1973).
[8] J. M. Kosterlitz and D. J. Thouless, J. Phys. C **7**, 1046 (1974).
[9] M. P. Gelfand and M. E. Fisher, Int. J. Thermophys. **9**, 713 (1988).
[10] K. Binder, in *Phase Transitions and Critical Phenomena*, edited by C. Domb and J. L. Lebowitz (Academic, New York, 1983), Vol. 8.
[11] M. P. Gelfand and M. E. Fisher, Physica A **166**, 1 (1990).
[12] D. Jasnow, in *Phase Transitions and Critical Phenomena*, edited by C. Domb and J. L. Lebowitz (Academic, New York, 1986), Vol. 10.
[13] P. Kleban, Phys. Rev. Lett. **67**, 2799 (1991).
[14] J. Adler, Phys. Rev. B **36**, 2473 (1987).
[15] M. Holzer and M. Wortis, Phys. Rev. B **40**, 11 044 (1989).
[16] L. J. Shaw and M. E. Fisher, Phys. Rev. A **39**, 2189 (1989).
[17] G. Münster, Nucl. Phys. **B324**, 630 (1989).
[18] Y. Ueno, G. Sun, and I. Ono, J. Phys. Soc. Jpn. **58**, 1162 (1989).
[19] C. Borgs and W. Janke, J. Phys. I (France) **2**, 2011 (1992).
[20] V. Privman, Phys. Rev. Lett. **61**, 183 (1988).
[21] V. Privman and N. M. Švrakić, Phys. Rev. Lett. **62**, 633 (1989).
[22] V. Privman and N. M. Švrakić, J. Stat. Phys. **54**, 735 (1989).
[23] K. K. Mon, S. Wansleben, D. P. Landau, and K. Binder, Phys. Rev. Lett. **60**, 708 (1988).
[24] K. K. Mon, S. Wansleben, D. P. Landau, and K. Binder, Phys. Rev. B **39**, 7089 (1989).
[25] H. Meyer-Ortmanns and T. Trappenberg, J. Stat. Phys. **58**, 185 (1990).
[26] M. Caselle, F. Gliozzi, and S. Vinti, Phys. Lett. **74**, B302 (1993).
[27] M. Hasenbusch and K. Pinn, Physica A **192**, 342 (1993); and (unpublished).
[28] B. Berg, U. Hansmann, and T. Neuhaus, Z. Phys. B **90**, 229 (1993).
[29] R. H. Swendsen and J. S. Wang, Phys. Rev. Lett. **58**, 86 (1987).
[30] B. A. Berg and T. Neuhaus, Phys. Rev. Lett. **68**, 9 (1992).
[31] M. P. Nightingale, in *Finite Size Scaling and Numerical Simulation of Statistical Systems*, edited by V. Privman (World Scientific, Singapore, 1990).
[32] J. M. Luck, J. Phys. (Paris) Lett. **42**, L275 (1981).
[33] L. Onsager, Phys. Rev. **65**, 117 (1944).
[34] D. B. Abraham, L. F. Ko, and N. M. Švrakić, J. Stat. Phys. **56**, 563 (1989).
[35] D. B. Abraham, N. M. Švrakić, and P. J. Upton, Phys. Rev. Lett. **68**, 423 (1992).
[36] D. B. Abraham and N. M. Švrakić, J. Stat. Phys. **63**, 1077 (1991).
[37] A few preliminary results of this study were summarized in M. A. Novotny, H. L. Richards, and P. A. Rikvold, in *Interface Dynamics and Growth*, edited by K. S. Liang, M. P. Anderson, R. F. Bruinsma, and G. Scoles, MRS Symposia Proceedings No. 237 (Materials Research Society, Pittsburg, 1992), p. 67.
[38] M. P. A. Fisher, D. S. Fisher, and J. D. Weeks, Phys. Rev. Lett. **48**, 368 (1982).
[39] G. Forgacs, R. Lipowsky, and Th. M. Nieuwenhuizen, in *Phase Transitions and Critical Phenomena*, edited by C.

Domb and J. L. Lebowitz (Academic, New York, 1991), Vol. 14.
[40]H. H. Roomany and H. W. Wyld, Phys. Rev. D **21**, 3341 (1980).
[41]M. N. Barber, in *Phase Transitions and Critical Phenomena*, edited by C. Domb and J. L. Lebowitz (Academic, New York, 1983), Vol. 8.
[42]H. A. Kramers and G. H. Montrol, Phys. Rev. **60**, 252 (1941).
[43]W. J. Camp and M. E. Fisher, Phys. Rev. B **6**, 946 (1972).
[44]K. Huang, *Statistical Mechanics* (Wiley, New York, 1963).
[45]M. A. Novotny, J. Math. Phys. **29**, 2280 (1988).
[46]A. Jennings, *Matrix Computation for Engineers and Scientists* (Wiley, London, 1977).
[47]D. B. Abraham, G. Gallavotti, and A. Martin-Löff, Physica **65**, 73 (1973).
[48]M. E. Fisher and A. E. Ferdinand, Phys. Rev. Lett. **19**, 169 (1967).
[49]R. L. Burden and J. D. Faires, *Numerical Analysis* (PSW-Kent, Boston, 1989).
[50]H. Wen and M. E. Fisher (private communication). These data were calculated using the methods indicated in Refs. 16 and 61 and numerical estimates of T_R, T_c, and certain critical exponents and amplitudes as referenced therein. Guidelines on accuracy are given in Ref. 61.
[51]J. J. Morris, J. Stat. Phys. **69**, 539 (1992).
[52]G. Münster, Nucl. Phys. **B386**, 701 (1992).
[53]V. Privman and M. E. Fisher, J. Stat. Phys. **33**, 385 (1983).
[54]J. M. Drouffe and C. Itzykson, *Statistical Field Theory* (Cambridge University Press, Cambridge, England, 1989).
[55]C. Itzykson and J. B. Zuber, Nucl. Phys. **B275**, 580 (1986).
[56]N. M. Švrakić, V. Privman, and D. B. Abraham, J. Stat. Phys. **53**, 1041 (1988).
[57]Equation (24) is written in Refs. 21 and 22 as $\kappa_L^{(+/-)}(T) = k_B T \frac{3}{2} \pi^2 \xi_L^{(+/-)}(T)/(L+\ell)^2$, with $\ell = 1$. However, an $O(1/L)$ correction proportional to $\kappa(T)$ arises if an arbitrary value ℓ is added to L in the denominator of Eq. (24) instead of the optimal value ℓ_0. Since $\kappa(T)$ is very large at low temperatures and diverges at $T = 0$, it is important to find ℓ_0. Our numerical calculations are consistent with $\ell_0 = 2$ at low temperatures for large systems. This gives the correlation length the same L-dependence in 2D as is given in 3D for $T < T_R$ [see Eq. (30)]. Even so, an $O(1/L)$ correction, which is not proportional to $\kappa(T)$ remains.
[58]P. E. Wolf *et al.*, J. Phys. (Paris) **46**, 1987 (1985).
[59]M. P. M. den Nijs, M. P. Nightingale, and M. Schick, Phys. Rev. B **26**, 2490 (1982).
[60]H. van Beijeren, Commun. Math. Phys. **40**, 1 (1975).
[61]M. E. Fisher and H. Wen, Phys. Rev. Lett. **68**, 3654 (1992).
[62]G. G. Cabrera and R. Jullien, Phys. Rev. Lett. **57**, 393 (1986).
[63]G. G. Cabrera and R. Jullien, Phys. Rev. B **35**, 7062 (1987).
[64]M. N. Barber and M. E. Cates, Phys. Rev. B **36**, 2024 (1987).
[65]H. Kitatani and T. Oguchi, J. Phys. Soc. Jpn. **57**, 1344 (1988).
[66]B. Dünweg, A. Milchev, and P. A. Rikvold, J. Chem. Phys. **94**, 3958 (1991).
[67]M. A. Novotny, in *Quantum Monte Carlo Methods in Equilibrium and Nonequilibrium Systems*, edited by M. Suzuki (Springer-Verlag, Berlin, 1986), Vol. 14.
[68]M. A. Novotny, J. Math. Phys. **20**, 1146 (1979).
[69]M. A. Novotny, J. Math. Phys. **29**, 2280 (1988).
[70]M. A. Novotny, Europhys. Lett. **17**, 297 (1992).
[71]M. A. Novotny, Phys. Rev. B **46**, 2939 (1992).
[72]P. Audit, J. Math. Phys. **32**, 561 (1991).
[73]J. H. Wilkinson, *The Algebraic Eigenvalue Problem* (Clarendon Press, Oxford, 1965).